Probing Spatial Correlations with Nanoscale Two-Contact Tunneling

Jeff M. Byers*
Department of Physics, University of California, Santa Barbara, California 93106

Michael E. Flatté
Division of Applied Sciences, Harvard University, Cambridge, Massachusetts 02138
(Received 22 February 1994)

Interference effects on the transport through two localized tunnel junctions on the surface of a well-grounded sample reveal intrinsic spatial correlations characteristic of the uncoupled sample. Differential conductances of the two-junction probe are related to the spatial correlations of both normal and superconducting samples. For a superconducting sample the gap anisotropy strongly affects the results. This may serve as a sensitive probe of the order parameter in high-temperature superconductors.

PACS numbers: 73.40.Gk, 73.50.–h, 74.50.+r

The advent of scanning tunneling microscopy (STM) has enabled the characterization of materials on the atomic scale through measurements of the local density of states (LDOS). Recently, in a series of STM experiments on a Cu(111) surface, the local electronic correlations of the surface-state electrons were probed through their influence on the LDOS around an Fe impurity [1]. Properties which might be determined from these types of measurements, but could not be probed by an STM measurement on the homogeneous sample, include the *angularly resolved* dispersion relations and mean free path, as well as the density of states as a function of energy *and* momentum.

In this type of STM experiment the characteristics of an impurity limit the information available on the local electronic correlations around it. In particular, the influence of the impurity is manifested in oscillations (of approximately the Fermi wavelength) in the LDOS. These short-distance oscillations allow accurate determination of the dispersion relations, but hinder measurements of long-distance properties. By replacing the impurity with a contact, and taking an appropriate differential conductance between the two contacts, one obtains a measurement which does not contain substantial oscillations, but reveals long-distance behavior.

A conceptually straightforward, but impractical, two-contact arrangement would consist of two STM tips which could be placed from 1 to 1000 Å apart. This would allow probing of correlations with short length scales (1−10 Å), such as Fermi wavelengths in desired directions, medium length scales (10−100 Å), such as high-T_c superconducting coherence lengths and charge-density wave oscillations, and long length scales (100−1000 Å), such as mean free paths, transitions from ballistic to diffusive propagation, low-T_c coherence lengths, and angularly anisotropic density-of-states effects [2].

Practical alternatives to the two-tip STM are possible. If a single small contact of size ~100 Å could be made on a surface, the other contact could be an STM. In some systems contact has been made to nanofabricated wires as small as 100 Å, fabricated using STM chemical vapor deposition [3] on a smooth surface. With such an arrangement at least the long-range correlations could be probed.

The two-contact experiment is also insensitive to a small concentration of impurities on the surface. Impurities would produce oscillations in the LDOS due to the scattering of electrons from one contact to the other. A contact detects an average of the LDOS over its area, so if the contact diameter is large compared to the Fermi wavelength these oscillations would be greatly suppressed.

The specific application we will focus on is detecting gap anisotropy in high-temperature superconductors. For a $d_{x^2-y^2}$ gap, which has four nodes, we find at voltages much less than the gap quasiparticles can only travel in the real-space directions roughly parallel to node momenta, yielding "channels" of conductance. At voltages slightly higher than the gap maximum there are more states for momenta near the gap maximum, so the channels would appear rotated by 45°. With a 100 Å contact and an STM tip 1000 Å away, the angular resolution would be 6°, similar to photoemission [4]. Major advantages over photoemission include the improved energy resolution and the ability to characterize the surface with the STM while performing the experiment. In contrast to other tunneling probes of gap anisotropy [5], the details of the tunnel barrier are not important.

Measurements of gap anisotropy promise to be effective in distinguishing among the various theories of high-temperature superconductivity, including phonon-mediated s-wave [6], antiferromagnetic-spin-fluctuation-mediated $d_{x^2-y^2}$ [7], anyonic $d_{x^2-y^2} + i\alpha d_{xy}$ [8] gaps. Despite evidence of a finite density of states at low energy [9], angular anisotropy of the gap [4], and changes of sign in the gap around the Fermi surface [5], evidence for d-wave superconductivity is not conclusive. Furthermore, even less evidence selects among the various forms of d-wave gaps.

Figure 1 shows the geometry of the two-contact probe. There are three reservoirs connected to a sample. One of the reservoirs is well connected to the sample and

 0031-9007/95/74(2)/306(4)$06.00

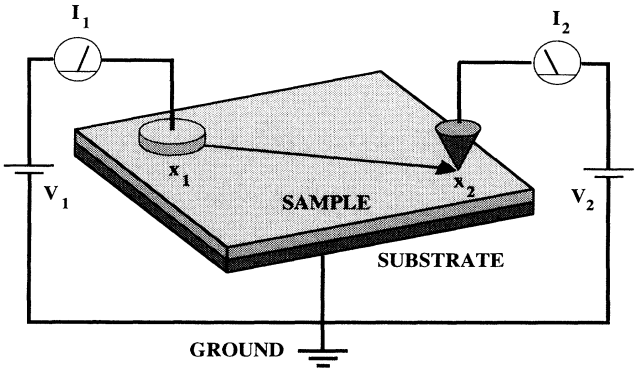

FIG. 1. Probe-sample geometry. The sample is strongly connected to ground and weakly connected to two localized junctions, at least one of which is mobile. The possibility considered in this Letter is a 100 Å nanofabricated contact for one localized junction (located at $\mathbf{x}_1$) and an STM tip for the other (located at $\mathbf{x}_2$).

acts as a ground that determines its chemical potential (this will be discussed more below). This configuration is intentionally different from the ungrounded, two-contact geometry relevant for quantum dots [10]. In this Letter the behavior of the homogeneous sample material is of interest—not the behavior of electrons confined to a small island. The remaining two reservoirs are weakly linked to the sample and act as tunnel junctions.

The Hamiltonian for the uncoupled system is

$$H_I = \sum_{\alpha_i} \epsilon_{\alpha_i} c^\dagger_{\alpha_i} c_{\alpha_i} + \int d\mathbf{x}\, d\mathbf{x}' \Big(\sum_s \epsilon(\mathbf{x},\mathbf{x}') \psi^\dagger_s(\mathbf{x}) \psi_s(\mathbf{x}') + [\Delta(\mathbf{x},\mathbf{x}') \psi^\dagger_\uparrow(\mathbf{x}) \psi^\dagger_\downarrow(\mathbf{x}') + \text{H.c.}] \Big), \quad (1)$$

where $c^\dagger_{\alpha_i}$ creates an electron in eigenstate α_i in lead $i = 1$, 2, or G (ground). The last terms describe the sample, and are written in coordinate representation in anticipation of a spatially inhomogeneous response to the localized tunneling probes. The transfer Hamiltonian is

$$H_T = \sum_{\alpha_i} \int d\mathbf{x} [W_{\alpha_i} v_i(\mathbf{x} - \mathbf{x_i}) \psi^\dagger(\mathbf{x}) c_{\alpha_i} + \text{H.c.}], \quad (2)$$

where $W_{\alpha_i} v_i(\mathbf{x} - \mathbf{x_i})$ is the amplitude for an electron in energy level α_i of lead i to jump to position $\mathbf{x}$ in the sample. $\mathbf{x}_i$ is the mean position of junction i. Since the ground is visualized as a broad contact, we assume for simplicity $v_G(\mathbf{x}) = v_G$. The functions $v_1(\mathbf{x})$ and $v_2(\mathbf{x})$ represent the geometry of the junction interfaces (acting to an extent as the wave function of an electron under the lead).

Each of the two localized junctions 1 and 2 has its own voltage difference with respect to ground (V_1 and V_2), as depicted in Fig. 1. The current through the junctions was calculated as a function of voltage and position:

$$\begin{aligned} I_1 = \frac{4e}{\pi\hbar} \int d\omega & [f_1^+(\omega)\{\Gamma_1 \mathrm{Im}(g^{\mathrm{ret}}(\mathbf{x}_1,\mathbf{x}_1)) + 2\Gamma_1^2[\mathrm{Im}(g^{\mathrm{ret}}(\mathbf{x}_1,\mathbf{x}_1))]^2\} + [f_1^+(\omega) + f_2^+(\omega)]\Gamma_1\Gamma_2[\mathrm{Im}(g^{\mathrm{ret}}(\mathbf{x}_1,\mathbf{x}_2))]^2 \\ & - [f_1^+(\omega) - f_2^+(\omega)]\Gamma_1\Gamma_2[\mathrm{Re}(g^{\mathrm{ret}}(\mathbf{x}_1,\mathbf{x}_2)) + [f_1^+(\omega) + f_1^-(\omega)]\Gamma_1^2[\mathrm{Im}(f^{\mathrm{ret}}(\mathbf{x}_1,\mathbf{x}_1))]^2 \\ & - [f_1^+(\omega) - f_1^-(\omega)]\Gamma_1^2[\mathrm{Re}(f^{\mathrm{ret}}(\mathbf{x}_1,\mathbf{x}_1)) + [f_1^+(\omega) + f_2^-(\omega)]\Gamma_1\Gamma_2[\mathrm{Im}(f^{\mathrm{ret}}(\mathbf{x}_1,\mathbf{x}_2))]^2 \\ & - [f_1^+(\omega) - f_2^-(\omega)]\Gamma_1\Gamma_2[\mathrm{Re}(f^{\mathrm{ret}}(\mathbf{x}_1,\mathbf{x}_2))]^2], \end{aligned} \quad (3)$$

where $g^{\mathrm{ret}}(\mathbf{x}_i,\mathbf{x}_j) = \int d\mathbf{x}\, d\mathbf{x}'\, v_i(\mathbf{x} - \mathbf{x}_i)\bar{g}^{\mathrm{ret}}(\mathbf{x},\mathbf{x}')v_j^*(\mathbf{x}' - \mathbf{x}_j)$, and $\bar{g}$ is the Green function of the uncoupled sample. f^{ret} is defined similarly. $f_i^{\pm}(\omega) = f(\omega \pm eV_i) - f(\omega)$, where $f(\omega)$ is the Fermi factor and $\Gamma_i = \pi \sum_{\alpha_i} |W_{\alpha_i}|^2 \delta(\omega - \epsilon_{\alpha_i})$. Each term in Eq. (3) can be obtained from a Fermi's golden rule calculation carried out to second order. Equation (3) represents several tunneling mechanisms [depicted in Figs. 2(a) and 2(b)] that combine wave function interference effects and transport. The first and second terms are direct electron tunneling (D) and reflection (R), respectively, at junction 1. These terms are not influenced by the second junction.

The second line of Eq. (3) is the influence of the other tunnel junction on the normal conduction channel (T). If this line is rearranged, the combination $f_1^+(\omega)\Gamma_1\Gamma_2\{[\mathrm{Im}(g^{\mathrm{ret}})]^2 - [\mathrm{Re}(g^{\mathrm{ret}})]^2\}$ represents an interference effect caused by the second junction as if it were a block of material on the surface of the sample with no external connection (this process is independent of eV_2). The remaining combination $f_2^+(\omega)\Gamma_1\Gamma_2\{[\mathrm{Im}(g^{\mathrm{ret}})]^2 + [\mathrm{Re}(g^{\mathrm{ret}})]^2\}$ represents transport between junctions 1 and 2 through the sample and is not present if $eV_2 = 0$.

The last two lines in Eq. (3) can also be rearranged into interference and transport terms in the same manner. The third line of Eq. (3) represents Andreév reflection [11] at junction 1 where an incident electron in the lead is reflected as a hole with a Cooper pair injected into the superconducting sample (AR) [12]. The last line in Eq. (3) represents a novel process where an incident electron at junction 1 is Andreév reflected, but the hole ends up in the opposing lead (AT). Alternatively, one can turn the reflected hole in junction 2 into another incident electron and visualize the process as each lead contributing an electron toward forming a Cooper pair in the sample. In order for this particular mechanism to contribute to the current the two junctions must be within a few superconducting coherence lengths of one another.

The Fermi's golden rule calculations are justified if the sample has a definite chemical potential. The grounding

lead produces this situation by inducing a lifetime $\Gamma_G^{-1} = [2\pi|W_G v_G|^2 N_G(0)]^{-1}$ for an electronic excitation to leave the system via the ground [where $N_i(0)$ is the density of states at the Fermi level of lead i]. In the situation we consider Γ_G is small enough not to affect local electronic transport, but large enough that any path from contact 1 to contact 2 which involves scattering off the sample boundaries is strongly suppressed. The grounding-lead lifetime differs from those due to intrinsic sample processes, such as inelastic scattering, which produce different electronic excitations in the sample. One needs only observe that in the ungrounded, two-contact geometry, the current through lead 1 must equal the current through lead 2, something not required for the grounded geometry.

To remove the effect of the position-independent background a cross-junction differential conductance can be defined by taking the derivative of I_1 with respect to the voltage V_2 across the other junction. Doing so yields the simpler result

$$R_Q \frac{d}{dV_2} I_1(\mathbf{x}_1, \mathbf{x}_2; V_2) = 4\Gamma_1\Gamma_2[|g^{\mathrm{ret}}(\mathbf{x}_1, \mathbf{x}_2; \omega = eV_2)|^2 - |f^{\mathrm{ret}}(\mathbf{x}_1, \mathbf{x}_2; \omega = eV_2)|^2], \quad (4)$$

where $R_Q \equiv \pi\hbar/e^2$. The relative sign beween the terms has its physical origin in the Andreév process (represented by $|f^{\mathrm{ret}}|^2$) which places a hole in the other lead, whereas the normal channel (represented by $|g^{\mathrm{ret}}|^2$) places an electron there, thus resulting in opposing currents. I_2 can be found by interchanging the labels 1 and 2 in I_1. Forming the combinations $I_T = (I_1 - I_2)/2$ and $I_G = I_1 + I_2$, different pieces of the Green functions can be measured:

$$R_Q \frac{d}{dV_2} I_T(\mathbf{x}_1, \mathbf{x}_2; V_2) = \sigma_{BT} + 4\Gamma_1\Gamma_2\{[\mathrm{Re}(g^{\mathrm{ret}}(\mathbf{x}_1, \mathbf{x}_2; \omega = eV_2))]^2 - [\mathrm{Im}(f^{\mathrm{ret}}(\mathbf{x}_1, \mathbf{x}_2; \omega = eV_2))]^2\},$$

$$\frac{R_Q}{2} \frac{d}{dV_2} I_G(\mathbf{x}_1, \mathbf{x}_2; V_2) = \sigma_{BG} + 4\Gamma_1\Gamma_2\{[\mathrm{Im}(g^{\mathrm{ret}}(\mathbf{x}_1, \mathbf{x}_2; \omega = eV_2))]^2 - [\mathrm{Re}(f^{\mathrm{ret}}(\mathbf{x}_1, \mathbf{x}_2; \omega = eV_2))]^2\}, \quad (5)$$

where σ_{BT} and σ_{BG} are position-independent background terms. Equations (4) and (5) demonstrate that this particular example of a nanofabricated probe can make direct measurements of spatial correlations due to electronic transport within the sample.

Figure 2(c) shows the distinction, for a quasi-two-dimensional system, between an isotropic superconductor's response and the normal state response in the cross-junction differential conductance. The bias is set just above the gap maximum, $eV = 1.1\Delta_0$. For this figure, to show the short-wavelength oscillatory behavior, we took $v_1(\mathbf{x}) = v_2(\mathbf{x}) = \delta(\mathbf{x})$. As the sample becomes superconducting the oscillations are enhanced due to the increased density of states just above $\omega = \Delta_0$. The wavelength of the rapid oscillation is set by k_F, and the asymptotic behavior is $1/\rho$ as expected for a 2D geometry. In a typical high-T_c superconductor, $k_F^{-1} \sim 1$ Å. A characteristic estimate of the magnitude of this conductance relative to the conductance through *one* of the contacts is $\Gamma N(0)$, where $N(0)$ is the (normal) sample's density of states. This is of the order of 1% for most systems and should therefore be visible. Essentially, there is no reason for the cross-junction conductance to be substantially weaker than any other second-order tunneling process. Many of these second-order processes, like Andreév processes within an ultrasmall junction [13], have been observed.

As a further application of Eq. (4) consider the case of two contacts on the surface of a superconducting film that has a gap anisotropy. They are within an elastic mean free path of one another so that the Green functions represent ballistic and not diffusive propagation. At helium temperatures the mean free path on a high-temperature superconductor is $10^3 - 10^4$ Å [14].

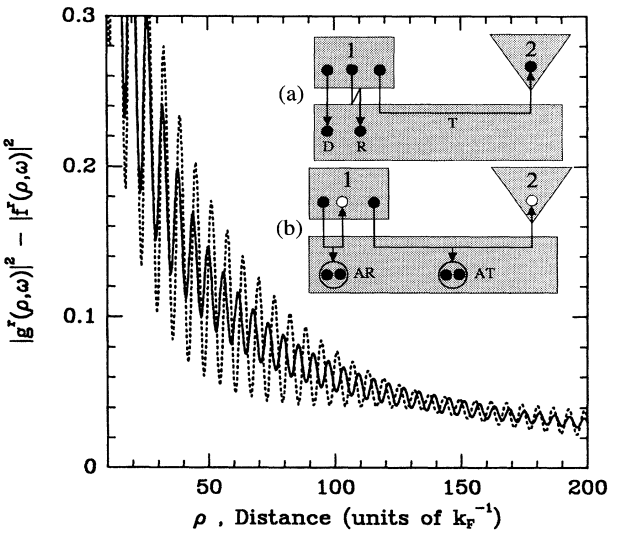

FIG. 2. Physical processes occurring in a two-junction geometry. (a) Schematic of normal state processes of direct (D) and reflected (R) tunneling between an electrode and the grounded sample. The process (T) is the interference and transport effect between the electrodes. (b) Schematic of anomalous processes in a superconducting sample where Andreév reflection occurs at one junction (AR) and both (AT). (c) Comparison of normal (solid line) and superconducting (dotted) state in the cross-junction differential conductance (defined in text) at a bias $eV = 1.1\Delta_0$. The superconducting gap $\Delta = 0.1\epsilon_F$ and is isotropic. [Differential conductance is in units of $4\Gamma_1 N(0)\Gamma_2 N(0) R_Q^{-1}$.]

Figure 3 shows the cross-junction differential conductance (multiplied by the radial distance ρ to allow easier visualization of the outlying regions) for an anisotropic superconductor as a function of x and y for the gap $\Delta_{\mathbf{k}} = \Delta_0 \cos(2\phi_{\mathbf{k}})$. $\phi_{\mathbf{k}}$ is the angle that the momentum $\mathbf{k}$ makes with the crystallographic a axis. The voltage bias is set well below the gap maximum ($eV = 0.1\Delta_0$) so that the quasiparticles are only able to propagate in the directions where $\Delta_{\mathbf{k}}$ has nodes.

One contact is 100 Å in diameter, and the other is atomic scale (an STM tip). To evaluate Eq. (4) under these conditions we take $v_1(\mathbf{x} - \mathbf{x}_1) = \theta(R - |\mathbf{x} - \mathbf{x}_1|)$ and $v_2(\mathbf{x} - \mathbf{x}_2) = \delta(\mathbf{x} - \mathbf{x}_2)$, where $R = 50$ Å. We calculated numerically the Green functions corresponding to a cylindrical Fermi surface because a sample of high-temperature superconductor would either be a thin film or a layered structure with weakly coupled planes. The rapid oscillations in the differential conductance on the scale of k_F^{-1} are gone, but the long-distance correlations are still visible. The dominant term from Eq. (4) is $|g^{\mathrm{ret}}(\mathbf{x}_1, \mathbf{x}_2; \omega = eV_2)|^2$ for $eV_2 \ll \Delta_0$. The terms $\mathrm{Re}(g^{\mathrm{ret}})$ and $\mathrm{Im}(g^{\mathrm{ret}})$ are very similar in appearance, therefore I_G and I_T look nearly identical to Fig. 3.

We note that for $eV > \Delta_0$ the enhanced density of states at the antinodes causes channels rotated by $\pi/4$ from the subgap result. These channels appear identical to those found in the impurity case [2], with the important exception that the short-wavelength oscillations present in the impurity case are absent here. Also, the signal in the two-contact experiment is substantially greater.

The primary goal of this Letter has been to offer an example of how two-contact localized spectroscopy can explore the spatial correlations of an uncoupled sample.

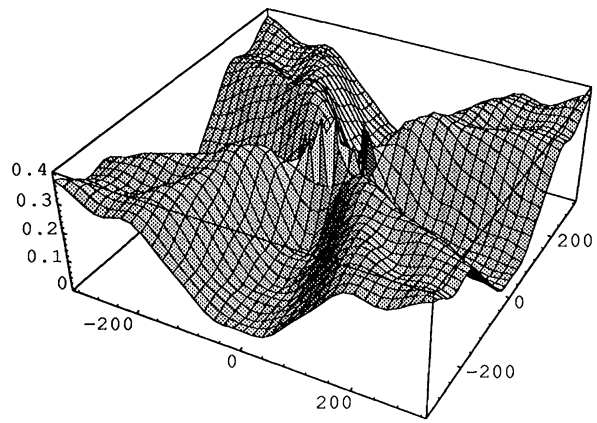

FIG. 3. Cross-junction differential conductance in position space (units of $k_F^{-1} \sim 1$ Å) multiplied by the radial distance ρ from the origin. A 100 Å diameter contact is located at the origin (indicated by the hole). The other contact is atomic scale (an STM tip). The function's value at a point indicates the cross-junction differential conductance when the STM tip is located there. The sample is a superconductor with the anisotropic gap $\Delta_{\mathbf{k}} = \Delta_0 \cos(2\phi_{\mathbf{k}})$ and $eV = 0.1\Delta_0$. The conductance is in units of $4\Gamma_1 N(0)\Gamma_2 N(0)(k_F R_Q)^{-1}$.

Tunneling with an STM measures the local density of states; however, our results indicate the possibility of probing *transport* phenomena via STM imaging of a 100 Å contact. Measuring gap anisotropy is merely one possible application of the ability to directly and in detail probe small-scale electronic transport. Analysis of angularly resolved mean free paths, the transition between ballistic and diffusive transport or the lifetimes of quasiparticles in both normal and superconducting samples should also be possible with nanoscale two-contact tunneling.

We acknowledge useful conversations with D. J. Scalapino and Y. Meir. J. M. B. was supported by NSF Grant No. DMR92-25027. M. E. F. acknowledges the support of JSEP through ONR N00014-89-J-1023.

Note added.—During revision we became aware of similar work [15].

*Present address: Code 6344, Naval Research Laboratory, Washington, DC 20375.

[1] M. F. Crommie, C. P. Lutz, and D. M. Eigler, Nature (London) **363**, 524 (1993).
[2] J. M. Byers, M. E. Flatté, and D. J. Scalapino, Phys. Rev. Lett. **71**, 3363 (1993).
[3] A. L. de Lozanne, E. E. Ehreichs, and W. F. Smith, J. Phys. Condens. Matter **5**, A409 (1993); E. E. Ehrichs, W. F. Smith, and A. L. de Lozanne, Ultramicroscopy **42–44**, 1438 (1992).
[4] B. O. Wells *et al.*, Phys. Rev. B **46**, 11 830 (1992); Z.-X. Shen *et al.*, Phys. Rev. Lett. **70**, 1553 (1993).
[5] D. A. Wollman *et al.*, Phys. Rev. Lett. **71**, 2134 (1993).
[6] G. M. Éliashberg, Zh. Eksp. Teor. Fiz. **38**, 966 (1960) [Sov. Phys. JETP **11**, 696 (1960)].
[7] N. E. Bickers, D. J. Scalapino, and S. R. White, Phys. Rev. Lett. **62**, 961 (1989); P. Monthoux and D. Pines, *ibid.* **69**, 961 (1992).
[8] D. S. Rokhsar, Phys. Rev. Lett. **70**, 493 (1993).
[9] W. N. Hardy *et al.*, Phys. Rev. Lett. **70**, 3999 (1993).
[10] Y. Meir and N. S. Wingreen, Phys. Rev. Lett. **68**, 2512 (1992).
[11] A. F. Andreév, Zh. Eksp. Teor. Fiz. **46**, 1823 (1964) [Sov. Phys. JETP **19**, 1228 (1965)].
[12] Recent theoretical [F. W. J. Hekking *et al.*, Phys. Rev. Lett. **70**, 4138 (1993)] and experimental [J. M. Hergenrother, M. T. Tuominen, and M. Tinkham, Phys. Rev. Lett. **72**, 1742 (1994)] investigations of Andreév scattering in normal-superconductor-normal systems have focused on small islands of low-temperature superconductor. Coulomb blockade plays a large role in the response of these systems, and gap anisotropy plays no role.
[13] For example, Y. De Wilde *et al.*, Phys. Rev. Lett. **72**, 2278 (1994).
[14] From microwave measurements the mean free path is 1.6 μm [D. A. Bonn *et al.*, Phys. Rev. B **47**, 11 314 (1993)]. Measurements of similar quality on $Bi_2Sr_2CaCu_2O_8$ have not been done, although regions of the surface without imperfections 500 Å $\times$500 Å are readily found with STM [C. K. Shih (private communication)].
[15] Q. Niu, C. Chang, and C. K. Shih, Phys. Rev. B (to be published).